

Efficient all-polymer solar cells based on thiazole-bridged middle band-gap polymer donor: The influence of alkyl side chain on polymer-polymer miscibility and photovoltaic performance

Zurong Du^{a,b}, Yongchao Zhang^a, Chunming Yang^{c,*}, Xunchang Wang^{a,b}, Dangqiang Zhu^a, Liangliang Han^a, Xichang Bao^{a,*}, Renqiang Yang^{a,*}

^a CAS Key Laboratory of Bio-based Materials, Qingdao Institute of Bioenergy and Bioprocess Technology, Chinese Academy of Sciences, Qingdao 266101, China

^b Center of Materials Science and Optoelectronics Engineering, University of Chinese Academy of Sciences, Beijing 100049, China

^c Shanghai Synchrotron Radiation Facility, Shanghai Institute of Applied Physics, Chinese Academy of Sciences, Shanghai 201204, China

ARTICLE INFO

Keywords:

Thiazole π bridge
Alkyl side chain
As-cast APSCs
Power conversion efficiency

ABSTRACT

In this work, three middle band-gap ($E_g \approx 1.70$ eV) polymer donors featuring thiazole moiety as π bridge while different alkyl side chain modification were synthesized for all-polymer solar cell (APSC) application. The influence of the configuration of alkyl side chain (linear, branched and alkylthio) on polymer-polymer miscibility and resulting photovoltaic performance was systemically investigated. The results indicated that the miscibility of polymer-polymer pair was sensitive to the solubility of resultant polymers, which was caused by diverse alkyl side chain modification. Since then, the most soluble one (P1, modified by 2-ethylhexyl side chain) could produce efficient as-cast APSC device with best PCE of 6.42%, accompanying with high V_{oc} of 0.88 V and J_{sc} of 14.22 mA cm^{-2} . This work revealed that while the incorporation of thiazole π bridge into quinoid-based polymer proves to be an efficient molecule design strategy, suitable alkyl side chain modification is also important to enhance polymer-polymer miscibility.

1. Introduction

Bulk-heterojunction polymer solar cells (BHJ-PSCs), with outstanding advantages of abundant raw material, light-weight and flexibility, exhibited great potential in printed electronics [1–4]. Among all kinds of BHJ-PSCs, all-polymer solar cells (APSCs), blending polymer donor and polymer acceptor in active layer, have drawn extensive research attention due to its excellent optical, thermal and mechanical stabilities [5,6]. However, the APSCs usually deliver lower power conversion efficiency (PCE) (normally $< 10\%$) than their polymer donor-small molecule acceptor counterparts. [7,8]. Especially for those based on ITIC derivatives, which reached the PCE over 16% [9,10]. The poor PCE of APSCs could be mainly ascribed to the non-optimal morphology of active layer. In general, the co-mixing of donor-acceptor is more difficult in the all-polymer system than that of polymer-small molecules system, which is easy to cause large phase separation in active layer, thus devastating the exciton dissociation process [11]. The miscibility of the polymer-polymer pair was closely related to their molecular structure. The optimization on molecular weight [12], planarity [13], and regularity [14] of polymers has made great progress,

indicating that the feature of main backbone could play an important role in determining the compatibility of polymer-polymer pairs. For the polymer with definite backbone structure, selecting suitable, flexible side chain is also significant, which could influence the intermolecular interactions, thus regulating the solubility, molecular stacking and charge transport [15,16]. Some successful examples involved in naphthalene diimide (NDI) based polymer acceptors have been reported, demonstrating the optimized BHJ morphology could be obtained via elaborately regulating the side chains, such as length [17], branch point [18], asymmetrical modification [19] or ternary polymerization [20]. The polymer with optimal alkyl side chain modification usually showed good miscibility, π -electron transport and light absorbance, resulting in high performance APSCs with increased short-circuit current (J_{sc}) and fill factor (FF). What's more, recent work focused on the novel polymer acceptor with isoindigo (IID) as electron deficient unit also demonstrated that the optimization on the length and amount of amide site appended alkyl side chain could greatly improve the PCE of APSCs. [21]. In that work, the side chain copolymerized one (2BO and 2HD ratio of 2:1) could provide excellent PCE of 7.3% with high J_{sc} of 13.2 mA cm^{-2} , more than 30% higher than the individual 2-butyltolyl

* Corresponding authors.

E-mail addresses: yangchunming@sinap.ac.cn (C. Yang), baoxc@qibebt.ac.cn (X. Bao), yangrq@qibebt.ac.cn (R. Yang).

<https://doi.org/10.1016/j.synthmet.2019.06.005>

Received 10 April 2019; Received in revised form 3 June 2019; Accepted 4 June 2019

Available online 07 June 2019

0927-7967/© 2019 Elsevier B.V. All rights reserved.

(2BO) or 2-hexyldecyl (2HD) modified counterparts. The excellent photovoltaic performance of the APSCs based on copolymers with optimized alkyl side chain could be mainly attributed to their moderate solubility, favorable BHJ morphology with optimal co-mixing state. In comparison to extensive efforts focused on the side chain engineering of polymer donor, relevant works concerning polymer acceptor are limited, which is also important in constructing highly-efficient single-junction APSC device. Notably, APSC with high PCE exceeding 10% has been achieved by tuning the side chain of polymer donor [22]. In brief, the optimization of alkyl side chain would be equally important in comparison to the main backbone regulation for the performance improvement of APSCs.

The quinoid-based polymer PCE10 (PTB7-Th) was one of the most efficient narrow band-gap polymer donor in APSCs. When paired with PNDIOD-T2 (commercial name: N2200), a high PCE of 5.73% has been obtained after film aging treatment (Table 2) [23]. However, the high lying highest occupied molecular orbit (HOMO) energy level, tedious synthesis procedure of fluorine-substituted thieno[3,4-*b*]thiophene-2-carboxylate unit and overlapped absorption spectrum with PNDIOD-T2 has restricted its application [24,25]. To overcome these defects, the thiazole bridged thieno[3,4-*b*]thiophene-2-carboxylate (Tz-2) unit was utilized as the candidate of the fluorine-substituted electron deficient (A) unit since this molecule design strategy made significant success in PSCs based on small molecules acceptors [26-28]. Considering the incorporation of strong electron affinity thiazole moiety into the A unit would improve the crystallinity of the backbone, long 2-octyldecane side chain was selected to ensure the solubility of polymer. Given these, in this work, the polymer with thiazole moiety as the electron-deficient π bridge into quinoid unit was firstly utilized in APSCs. Three different kinds of alkyl side chain (linear (dodecane), branched (2-ethylhexyl) and alkylthio (dodecane thio)) were selected as the modification moieties of the electron donating (D) unit to investigate their influence on polymer-polymer miscibility in APSC device. The results revealed that the configuration of alkyl side chains has significant influence on solubility, polymer-polymer miscibility and resultant photovoltaic performance of the three polymer donors. Among them, the one with branched alkyl side chain modification (P1) showed best miscibility with PNDIOD-T2. As a result, APSCs based on P1 delivered high PCE of 6.42%, which is significantly higher than that of PCE10. It should be noted that the best PCE in this work were obtained based on as-cast device, which is beneficial for large area fabrication.

2. Experimental

2.1. Device fabrication

The APSC device was fabricated adopting the conventional structure of ITO/PEDOT:PSS/ active layer /PFN/Al. The fabricating procedure was as follows: ITO glass substrates were cleaned via ultrasonic with detergent, deionized water, acetone, deionized water, isopropyl alcohol in sequentially for 15 min. After dried by ultrapure N_2 , the ITO-coated

glass substrates were treated with O_2 plasma for 6 min, spin-coated of a ~ 30 nm PEDOT:PSS on the ITO at 4000 rpm, and then baked at $150^\circ C$ for 20 min in an oven. Afterwards, the substrates were transferred into glove box, the active layer of polymer donor and PNDIOD-T2 was spin-coated onto the PEDOT:PSS film at 1400-1600 rpm for 60 s from CB solution at room temperature ($20^\circ C$). The optimized concentration of the blend solution was 12 mg/mL and the optimized mass ratio was 1:1. Subsequently, an ultrathin layer of PFN (4 nm, 0.2 mg/mL in methanol and 3 vol.% acetic acid) was spin-coated on the active layer under 2000 rpm for 20 s. Finally, Al (100 nm) metal electrode was thermally evaporated below 4×10^{-4} Pa. The device area was 10 mm^2 defined by a shadow mask.

2.2. Instruments and characterization

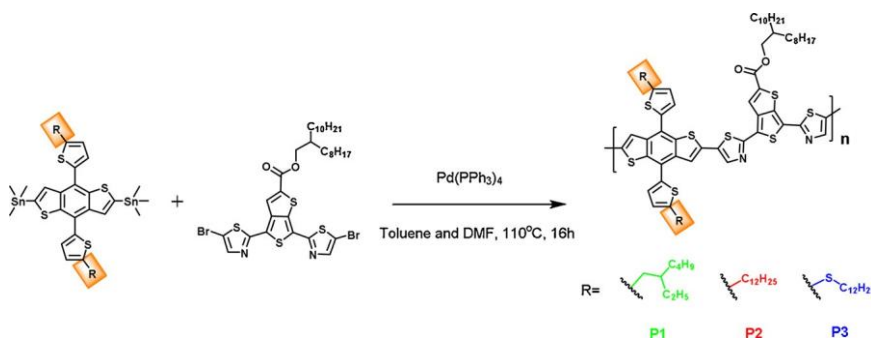
The *J-V* curves of APSC devices were tested using a Keithley 2400 source meter under an AM1.5 G solar simulator (Newport model 91160-1000). The light intensity was 100 mW cm^{-2} calibrated by a monosilicon detector including a KG-5 visible color filter. The EQE spectra were collected on a certified Newport incident photon conversion efficiency (IPCE) measurement system. The thickness of films was determined using a Dektak 150 surface profile meter. The UV-vis absorption spectra were recorded on a Lambda 25 spectrophotometer. The test solutions contained 10^{-5} M repeating unit of a polymer molecule in CB solution and the thin films were spin-coated from 12 mg/mL CB solution onto a quartz glass.

Grazing incidence wide-angle X-ray scattering (GIWAXS) patterns were collected by the beamline BL16B1 work-station (Shanghai Synchrotron Radiation Facility, China). The X-ray wavelength was 0.124 nm ($E = 10 \text{ KeV}$), and the incidence angle was set to 0.2° . All films were prepared under the same conditions with active layer preparation except adopting monocrystalline silicon wafer as substrate candidate. The background was deducted from the vacant silicon substrate. Photoluminescence (PL) spectra measurement was conducted on a Hitachi F-4600 fluorescence spectrophotometer equipped with a 150 W, ozone-free Xe lamp. The PMT Voltage was fixed on 800 V. The details of other measurements were described in Supporting Information (SI).

3. Results and discussion

3.1. Polymer characterization

The polymers were synthesized via Stille-coupling polymerization (Scheme 1) and all obtained polymers were purple-dark solid with good yield approaching to 80% (details in S1). The molecular weight was measured via high temperature ($150^\circ C$) gel permeation chromatography using 1,2,4-trichlorobenzene as eluent. The three polymers have similar number average molecular weight (M_n) of 19.3 kDa, 17.6 kDa and 15.1 kDa, respectively. The absorption spectra were plotted to calculate the solubility of the polymers based on the hypothesis that the absorbance intensity of a polymer in dilute solution is proportional to



Scheme 1. Synthetic routes of the polymer donors of P1, P2 and P3.

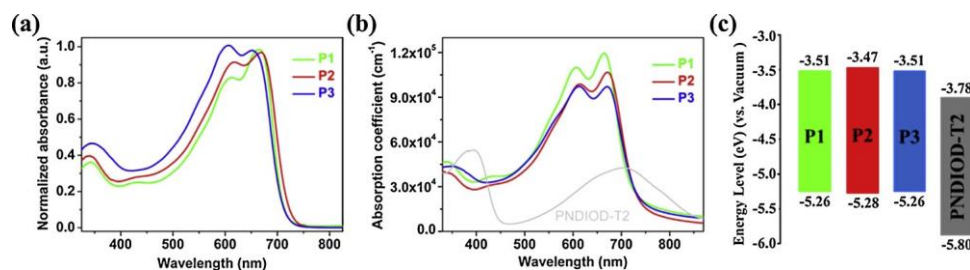


Fig. 1. The normalized absorbance spectra in CB (a) and thin film (b); (c) energy levels.

its mass concentration (details in S2). The average solubilities of the three polymers in CB were calculated as 13.2 mg mL^{-1} , 12.4 mg mL^{-1} and 10.4 mg mL^{-1} respectively. The solubility variation tendency of the polymers is closely related to different solubilizing ability of alkyl side chains [29,30]. As expected, the different solubility of the three polymers would have profound influence on their film formation property, the features of BHJ morphology, and photovoltaic performance of APSC devices.

3.2. Optical and electrochemical properties

The absorption spectra of P1, P2 and P3 in dilute CB and in thin film were shown in Fig. 1(a) and (b). The three polymers exhibit saddle-shaped absorbance profiles with intense absorbance band in the wavelength region from 550 nm to 690 nm, which forms good complementary absorption with the polymer acceptor PNDIOD-T2 in the Vis-NIR region (300–850 nm). The maximum absorption coefficients in thin film for the three polymers are around $1.0 \times 10^5 \text{ cm}^{-1}$ ($1.20 \times 10^5 \text{ cm}^{-1}$ for P1, $1.07 \times 10^5 \text{ cm}^{-1}$ for P2 and $9.72 \times 10^4 \text{ cm}^{-1}$ for P3), the small difference is probably caused by the difference of molecular weight [18,31]. The representative absorbance data of the three polymers are summarized in Table 1. The optical band gap (E_g^{opt}) of the three polymers calculated from the thin film absorbance are 1.71 eV, 1.68 eV and 1.67 eV, respectively, which are much larger than that of PCE10 (1.58 eV). This could be ascribed to the strong electron pulling property of thiazole moiety. From dilute CB to solid film, the absorbance profiles of the three polymers are similar with a slight red-shift (less than 30 nm), indicating strong aggregation property of the polymers, mainly attributed to good planarity of the backbone [26]. In addition, the absorbance profiles in both dilute solution and thin film of the three polymers show small deviation in relative to each other, indicating that the absorbance behavior mainly occurs in the conjugated backbone, thus little influenced by the variation of alkyl side chain. The energy levels were measured via cyclic voltammetry (details in S3). As shown in Fig. 1(c), the three polymers have almost same energy levels for both lowest unoccupied molecular orbit (LUMO) levels and highest occupied molecular orbit (HOMO) levels with small deviation less than 0.04 eV, implying the diverse alkyl side chains of these polymers also have little influence on the electron orbit distribution even for that of alkylthio substitution [32]. In addition, the offsets for both HOMO and LUMO energy levels between polymer donors and PNDIOD-T2 are larger than 0.27 eV, forming cascade energy level alignment for

efficient exciton dissociation [33]. The optical and electrochemical measurements indicated that diverse alkyl side chain substitution has neglect influence on the absorption property and energy levels of the three polymers.

3.3. Film characterization

It has been reported that the property of alkyl side chain can influence the molecule stacking, which would impact the mixing of polymers in the film [12,34]. Herein, the molecule stacking properties of the three polymers were characterized via GIWAXS measurement. The GIWAXS patterns and the corresponding line cutting profiles of the pristine polymer films are presented in Fig. 2(a)–(e). The three neat polymer films show strong (010) π - π stacking peak in out-of-plane direction at $q \approx 17.10 \text{ nm}^{-1}$ in comparison to relatively weak π - π stacking signal in in-plane direction, indicating dominating face-on orientation relative to the substrate, which is beneficial for π -electron transport. Despite the similar π - π stacking characteristic, the three polymers exhibit distinctive lamellar stacking in out-of-plane direction. The (100) stacking peaks for the three polymers are at $q \approx 2.50 \text{ nm}^{-1}$, 2.32 nm^{-1} and 1.90 nm^{-1} , corresponding to the lamellar stacking distance ($2\pi/q$) of 2.51 nm, 2.71 nm and 3.31 nm, respectively, which is consistent with the variation tendency of the length of the alkyl side chain. Even though, the branched 2-ethylhexyl chain showed best solubility. Interestingly, P1 based film has very similar lamellar stacking distance with that of PNDIOD-T2 ($q \approx 2.52 \text{ nm}^{-1}$), which could be beneficial for polymer-polymer co-mixing [35]. It should be noted that although there is long branched 2-octyldodecyl side chain append on the A unit, the lamellar stacking characteristic of the three polymers is sensitive to the property of the alkyl side-chains appended on the D unit, which is likely to suggest the severe distortion or good interdigitation arrangement of the long 2-octyldodecyl chain [36].

3.4. Photovoltaic performance

The photovoltaic performance of APSC devices were characterized with a conventional device structure. The J - V curves were depicted in Fig. 3(a) and the photovoltaic parameters were summarized in Table 2. Among the three polymers, the P1 based device exhibits best PCE of 6.42% with $V_{oc} = 0.88 \text{ V}$, $J_{sc} = 14.22 \text{ mA cm}^{-2}$, and FF = 51.38%. In comparison, the P2 based device shows slightly increased V_{oc} of 0.90 V, which can be attributed to little down-shift of HOMO energy level. Even

Table 1
Molecular weight, solubility, absorbance property, and energy level of the three polymers.

Polymer	M _w (kDa)	M _w /M _n	Solubility (mg mL ⁻¹)	λ_{max} (nm)		$E_g^{\text{opt a}}$ (eV)	$E_{\text{onset}}^{\text{ox b}}$ (V)	HOMO ^b (eV)	$E_{\text{onset}}^{\text{red b}}$ (V)	LUMO ^b (eV)
				Solution	Film					
P1	19.3	2.7	13.6	611, 664	606, 665	1.71	0.89	-5.26	-0.86	-3.51
P2	17.6	3.1	12.4	617, 668	613, 671	1.68	0.91	-5.28	-0.90	-3.47
P3	15.1	3.8	10.4	606, 652	612, 671	1.67	0.89	-5.26	-0.86	-3.51

^a Calculated from $E_g^{\text{opt}} = 1240/\lambda_{\text{onset}}^{\text{film}}$ (eV).

^b Calculated from the cyclic voltammograms. $E_{\text{onset}}^{\text{ox}}$ and $E_{\text{onset}}^{\text{red}}$ are the onset oxidation and reduction potentials.

Table 2
Photovoltaic properties, mobility and film thickness of P1, P2, P3 and PCE10 based APSC devices with PNDIOD-T2 as polymer acceptor.

Blend film	V_{oc} (V)	J_{sc}^a (mA cm^{-2})	FF (%)	PCE ^b (%)	μ_h ($\text{cm}^2 \text{V}^{-1} \text{s}^{-1}$)	μ_e ($\text{cm}^2 \text{V}^{-1} \text{s}^{-1}$)	Thickness ^c (nm)
P1	0.88 (0.88 ± 0.01)	14.22(13.93) (14.00 ± 0.25)	51.38 (51.61 ± 0.38)	6.42 (6.35 ± 0.2)	3.85×10^{-4} –	3.21×10^{-5} –	106 –
P2	0.90 (0.90 ± 0.01)	13.46(13.49) (13.61 ± 0.17)	50.51 (50.15 ± 0.44)	6.12 (6.11 ± 0.1)	2.78×10^{-4} –	2.72×10^{-5} –	114 –
P3	1.01 (1.00 ± 0.01)	2.34(2.46) (2.46 ± 0.19)	44.18 (44.07 ± 0.41)	1.04 (1.02 ± 0.2)	1.64×10^{-4} –	1.73×10^{-5} –	100 –
PCE10 ^d	0.79	13.00	55.60	5.73	3.40×10^{-4}	3.60×10^{-4}	100 ± 10

^a The data in parentheses is the integral current density from the EQE spectrum.

^b The second column is the average values obtained from 10 devices.

^c Thickness of the active layer.

^d The data is from reference [23].

so, the increase of V_{oc} can't compensate the loss of J_{sc} and FF, as the result to the decrease of PCE to 6.12%. However, the P3 based device exhibits severe PCE decrease to only 1.04%, which can be attributed to the extremely low J_{sc} of 2.34 mA cm^{-2} and FF of 44.18%. The external quantum efficiency curves (Fig. 3(b)) matched well with the absorbance spectra of the polymers and the integral current densities are less than 3% mismatch with the measured J_{sc} (Table 2). The photovoltaic performance testing results indicate that the J_{sc} , FF and resultant PCE are positively related to the solubilizing property of the three alkyl side chains. It should be noted that the V_{oc} of P3 based device is 0.1 V higher than that of P2 based device, which can be attributed to the electron pulling property of alkylthio substitution [37]. In addition, the device performance with active layer treated with DIO or thermal annealing were also measured (Table S1), which show some certain decrease compared to the as-cast devices. Although the demands on molecule structure for efficient as-cast APSC device are still unclear, it has been reported that complex film post-treatment processes are not compatible with the simple, low-cost and industrial-scale production demand of OPV module [38].

3.5. Charge generation, recombination and extraction

The different photovoltaic performance of the three polymers induced by different alkyl side chains reflects their inherent otherness of photoelectric conversion processes, which requires photoelectric kinetics investigation. Initially, the PL quenching behavior was evaluated via film emitting spectrum measurement. As can be observed from Fig. 4(a)-(c), the three neat polymer donor films have intensive PL emitting band ranged from 650 nm to 880 nm with around 20 nm red-shift in relative to their absorbance band. After blending with the polymer acceptor (PNDIOD-T2), the P1- and P2-based blend films exhibit high PL quenching rate (PLQR, calculated from the area rate of PL

emitting spectrum) approaching to 90% (89.4% for P1 and 86.0% for P2), revealing efficient exciton dissociation due to fine polymer-polymer co-mixing [39]. In comparison, the PLQR of P3-based blend film (64.8%) is significantly low, probably caused by remarkably reduced polymer-polymer contact. In further, the photocurrent density (J_{ph}) dependence on the effective voltage (V_{eff}) was measured to investigate the exciton dissociation and charge transport properties of the devices, where $J_{ph} = J_L - J_D$, J_L and J_D are current density under illumination and dark condition, respectively; $V_{eff} = V_{bi} - V_{appl}$, V_{bi} is the voltage when $J_{ph} = 0$, and V_{appl} is the applied voltage [40]. As shown in Fig. 4(d), the J_{ph} of P1 and P2 based devices improve linearly with V_{eff} until 1.6 V, suggesting incremental exciton dissociation. When V_{eff} exceeded the threshold of 1.6 V, the J_{ph} reach saturation. The saturated J_{ph} ($V_{eff} = 1.6 \text{ V}$) of P2 based device is 14.38 mA cm^{-2} , a little lower than that of P1 based device (15.73 mA cm^{-2}), which agrees well with the J_{sc} measured from J - V curves. In comparison, the J_{ph} of P3 based device can't reach saturation even at a high V_{eff} over 5 V, indicating relatively low exciton dissociation efficiency. In addition, a power-law dependent J_{sc} on light intensity (P) was investigated, which can be expressed as $J_{sc} \propto P^\alpha$, where α is power-component. The α approaching 1 indicates that the bimolecular recombination was negligible in the device [41]. All of the three devices show some degree of bimolecular recombination with α of 0.99, 0.98 and 0.96, respectively (Fig. 4(e)). The results discussed above suggest that the difference in photovoltaic performance for the three polymers as listed in Table 2 is mainly caused by distinct exciton dissociation process.

The charge mobility of the APSC devices was tested by space charge limited current (SCLC) model (the details are presented in S4). The pristine and fitting curves of hole and electron mobility were presented in Fig. 5(a) and (b), and the mobility values are also listed in Table 2. The hole mobility of P1, P2 and P3 based devices are 3.85×10^{-4} , 2.78×10^{-4} , $1.64 \times 10^{-4} \text{ cm}^2 \text{V}^{-1} \text{s}^{-1}$, respectively, which are very

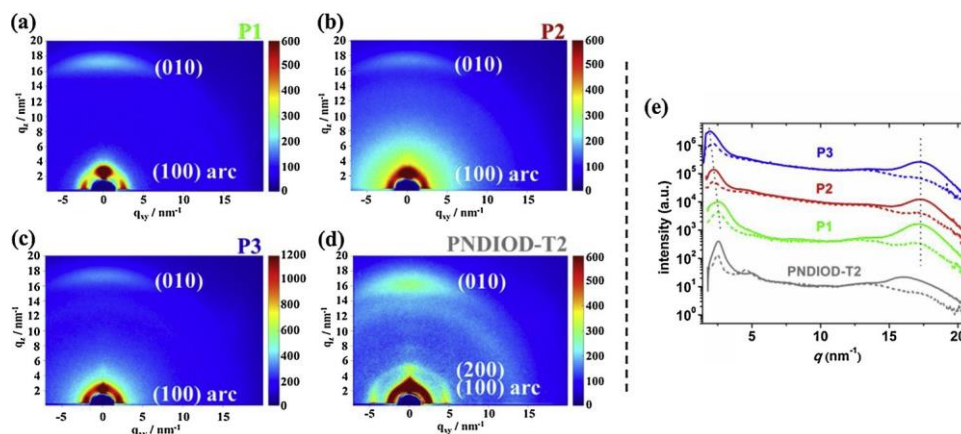


Fig. 2. The GIWAXS patterns of neat polymer films (a)-(d); and (e) the out-of-plane (solid line) and in-plane (dashed line) line cutting profiles.

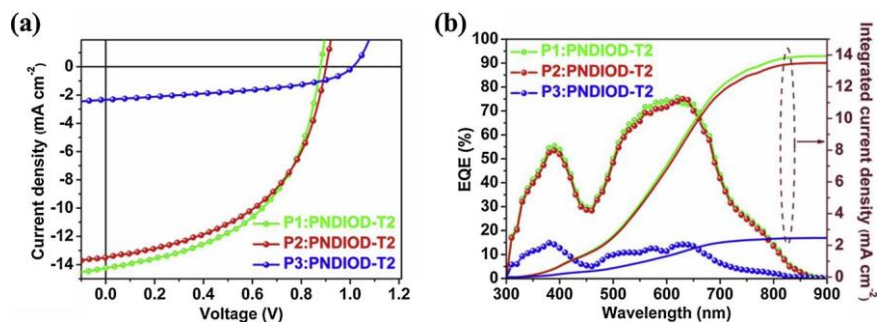
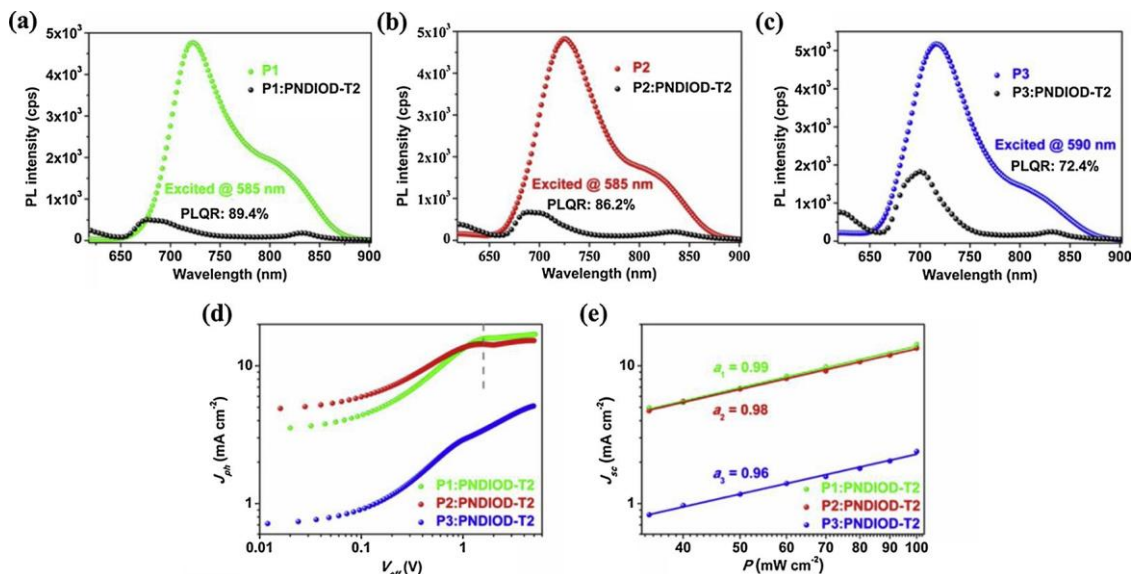
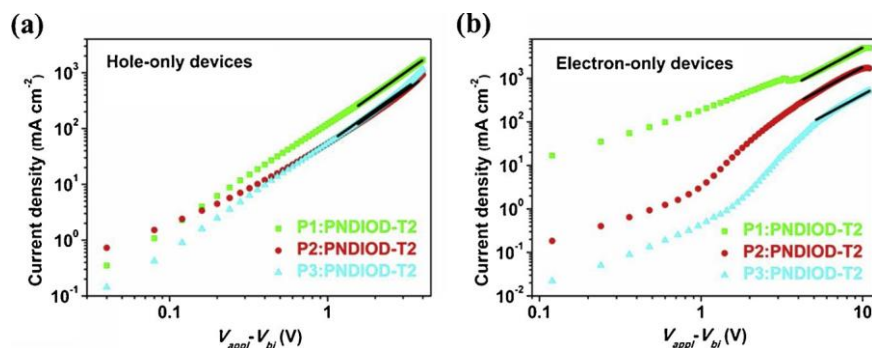
Fig. 3. (a) J - V curves, and (b) EQE and corresponding integral current density curves.Fig. 4. The PL spectra of neat and co-mixing films: (a) P1, (b) P2, and (c) P3; and (d) J_{ph} - V_{eff} curves; (e) J_{sc} - P curves.

Fig. 5. (a) hole-only and (b) electron-only SCLC curves.

close to that of P1 based device adopting PC₇₁BM or ITIC as acceptor (reference 16 and 17), suggesting fine crystallinity of the three polymers in active layer. However, the electron mobilities for the three devices (3.21×10^{-5} , 2.72×10^{-5} and 1.73×10^{-5} cm² V⁻¹ s⁻¹) are exactly one order of magnitude low in relative to those of the hole mobilities. The imbalance between hole and electron mobility would cause charge recombination, accounting for relatively low FF less than 60% [42]. In addition, the different charge mobility of the devices based on the three polymers reflects their different morphology in active layers. As a result, P1 based device exhibits the most desirable morphology, thus beneficial for efficient charge transport.

3.6. Morphology characterization

The GIWAXS patterns of the co-mixing films were recorded to investigate the molecular stacking characteristics in active layer (Fig. 6(a)-(d)). The three co-mixing films exhibit same (010) stacking peak at $q \approx 16.60$ nm⁻¹, corresponding to the π - π stacking distance of 0.378 nm. The π - π stacking distance is a little larger than that of the neat polymer films (0.367 nm), probably caused by the incorporation of PNDIOD-T2, which could increase the disorder of the co-mixing films. On the other hand, the q values of (100) stacking peak of P1 and P2 based co-mixing films are at 2.51 nm⁻¹ and 2.35 nm⁻¹ in both out-of-plane and in-plane directions, very close to those of the mean values of the neat polymer film stacking between polymer donor ($q \approx 2.50$ nm⁻¹

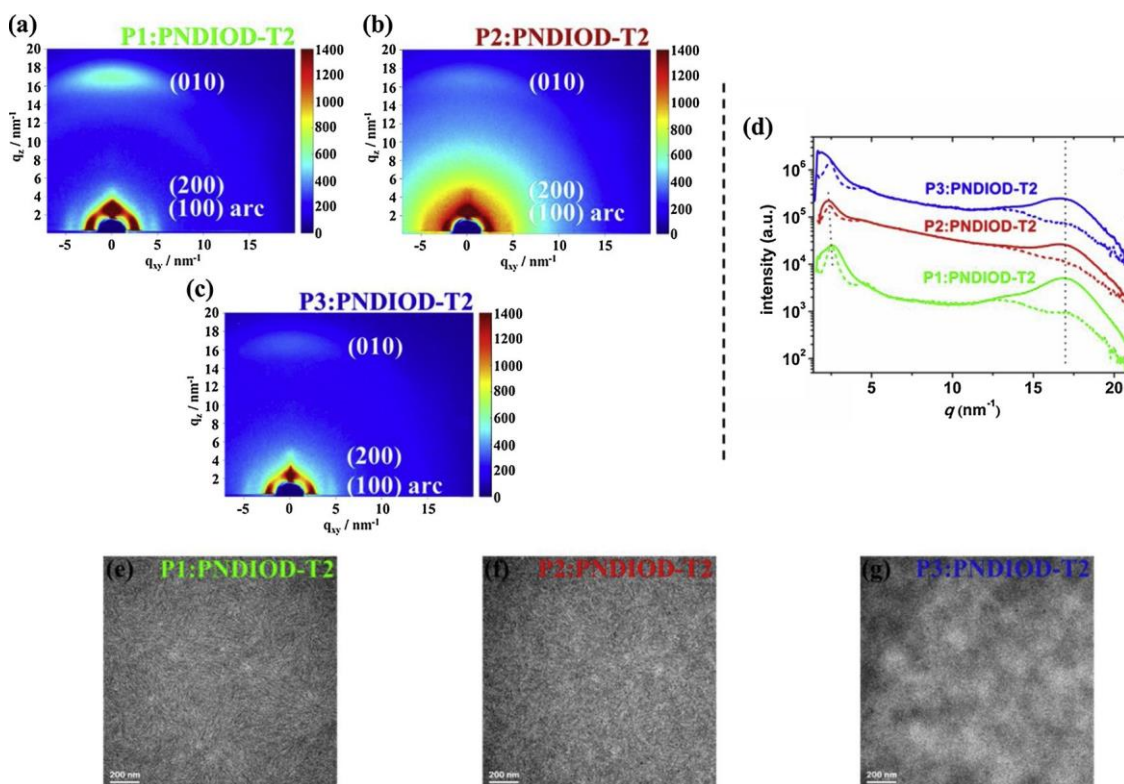


Fig. 6. The GIWAXS patterns: (a)-(c); and (d) the out-of-plane (solid line) and in-plane (dashed line) line cutting profiles; and TEM photographs (e)-(g) of the co-mixing films.

and 2.32 nm^{-1}) and PNDIOD-T2 ($q \approx 2.52 \text{ nm}^{-1}$). The mean effect of π - π stacking and lamellar stacking could imply good polymer-polymer alloying [43], which is necessary for efficient exciton dissociation. On the contrary, the P3 based co-mixing film exhibits two separated (100) stacking signals in out-of-plane direction and in-plane direction, respectively. Since the q value of (100) stacking peak in out-of-plane direction is around 2.48 nm^{-1} , approaching to that of the neat film of PNDIOD-T2, the (100) stacking in in-plane direction exhibits large amount of disorder, with q value lower than the detection limit (1.80 nm^{-1}). This mismatched lamellar stacking property in the two directions probably suggests relatively low blending degree between P3 and PNDIOD-T2 in the active layer [44].

The morphology of active layer films were further detected using TEM measurement (Fig. 6(e)-(g)). It can be observed that the P1 and P2 based co-mixing films have formed ordered fibrous network structure with around 10-20 nm domain size, which is desired for efficient exciton dissociation and charge transport [45]. In comparison, the P3 based film exhibits large amount of large size aggregation at the scale of 10^2 nm , implying excessive phase separation to restrict exciton dissociation [46]. Combined GIWAXS and TEM measurements, P3-based device have poorly mixed active layer morphology, thus greatly hinder its photovoltaic performance.

4. Conclusion

In summary, the influence of different alkyl side chains (linear, branched, alkylthio) on the solubility, miscibility and resultant photovoltaic performance of thiazole bridge-linked polymer donors were systematically investigated in APSCs. The results indicate that the photovoltaic performance is sensitive to the solubility of the polymer and the miscibility of the polymer-polymer pair. Among the three polymers, the 2-ethylhexyl modified one (P1) has best solubility and the most approximate lamellar aggregation size (2.51 nm) with that of the polymer acceptor PNDIOD-T2 (2.49 nm). As a result, P1 based APSC

device could produce highest PCE of 6.42% with large V_{oc} of 0.88 V, J_{sc} of 14.22 mA cm^{-2} and FF of 51.38%. In comparison, the P2 and P3 based APSC devices exhibit decreased photovoltaic performance in different degrees, which can be attributed to restricted exciton dissociation and charge transport caused by reduced miscibility with PNDIOD-T2. This work reveals that when pairing a polymer with its acceptor or donor counterpart, elaborate alkyl side chain modification is necessary to enhance the polymer-polymer miscibility.

Acknowledgments

This work was supported by the National Natural Science Foundation of China (51873227, 21604092, 11405259, 51573205 and 51503219), and Qingdao Applied and Fundamental Research (16-5-1-94-jch) for financial support. X. Bao thanks the Youth Innovation Promotion Association CAS (2016194) for financial support. The authors thank beamline BL16B1 (Shanghai Synchrotron Radiation Facility) for providing beam time.

Appendix A. Supplementary data

Supplementary material related to this article can be found, in the online version, at doi:<https://doi.org/10.1016/j.synthmet.2019.06.005>.

References

- [1] X. Gu, Y. Zhou, K. Gu, T. Kurosawa, Y. Guo, Y. Li, H. Lin, B.C. Schroeder, H. Yan, F. Molina-lopez, C.J. Tassone, C. Wang, S.C. Mannsfeld, H. Yan, D. Zhao, M.F. Toney, Z. Bao, *Adv. Energy Mater.* 7 (2017) 1602742.
- [2] L. Lu, T. Zheng, Q. Wu, A.M. Schneider, D. Zhao, L. Yu, *Chem. Rev.* 115 (2015) 12666-12731.
- [3] J. Li, Y. Wang, Z. Liang, N. Wang, J. Tong, C. Yang, X. Bao, Y. Xia, *ACS Appl. Mater. Interfaces* 11 (2019) 7022-7029.
- [4] Y. Liu, J. Lin, X. Che, Y. Qu, F. Liu, L. Liao, S.R. Forrest, *J. Am. Chem. Soc.* 139 (2017) 17114-17119.

- [5] Y. Diao, Y. Zhou, T. Kurosawa, L. Shaw, C. Wang, S. Park, Y. Guo, J.A. Reinspach, K. Gu, X. Gu, B. Tee, C. Pang, H. Yan, D. Zhao, M. Toney, S. Mannsfeld, Z. Bao, *Nat. Commun.* 6 (2015) 7955.
- [6] Y. Xu, J. Yuan, S. Zhou, M. Seifrid, L. Ying, B. Li, F. Huang, G.C. Bazan, W. Ma, *Adv. Funct. Mater.* 29 (2019) 1806747.
- [7] Z. Li, L. Ying, P. Zhu, W. Zhong, N. Li, F. Liu, F. Huang, Y. Cao, *Energy Environ. Sci.* 12 (2019) 157.
- [8] B. Guo, W. Li, G. Luo, X. Guo, H. Yao, M. Zhang, J. Hou, Y. Li, W.Y. Wong, *ACS Energy Lett.* 3 (2018) 2566-2572.
- [9] J. Yuan, Y. Zhang, L. Zhou, G. Zhang, H.L. Yip, T.K. Lau, X. Lu, C. Zhu, H. Peng, P.A. Johnson, M. Leclerc, Y. Cao, J. Ulanski, Y. Li, Y. Zhou, *Joule* 3 (2019) 1-12.
- [10] B. Fan, D. Zhang, M. Li, W. Zhong, Z. Zeng, L. Ying, F. Huang, Y. Cao, *Sci. China Chem.* (2019), <https://doi.org/10.1007/s11426-019-9457-5>.
- [11] G. Wang, F.S. Melkonyan, A. Facchetti, T.J. Marks, *Angew. Chem. Int. Ed.* 58 (2019) 4129-4142.
- [12] H. Kang, M.A. Uddin, C. Lee, K.H. Kim, T.L. Nguyen, W. Lee, Y. Li, C. Wang, H.Y. Woo, B.J. Kim, *J. Am. Chem. Soc.* 137 (2015) 2359-2365.
- [13] Y. Guo, Y. Li, O. Awartani, J. Zhao, H. Han, H. Ade, D. Zhao, H. Yan, *Adv. Mater.* 28 (2016) 8483-8489.
- [14] Z. Li, X. Xu, W. Zhang, X. Meng, W. Ma, A. Yartsev, O. Inganäs, M.R. Andersson, R.A. Janssen, E. Wang, *J. Am. Chem. Soc.* 138 (2016) 10935-10944.
- [15] J. Mei, Z. Bao, *Chem. Mater.* 26 (2014) 604-615.
- [16] H. Yao, L. Ye, H. Zhang, S. Li, S. Zhang, J. Hou, *Chem. Rev.* 116 (2016) 7397-7457.
- [17] W. Lee, C. Lee, H. Yu, D.J. Kim, C. Wang, H.Y. Woo, J.H. Oh, B. Kim, *Adv. Funct. Mater.* 26 (2016) 1543-1553.
- [18] H. You, D. Kim, H.H. Cho, C. Lee, S. Chong, N.Y. Ahn, M. Seo, J. Kim, F.S. Kim, B.J. Lim, *Adv. Funct. Mater.* 28 (2018) 1803613.
- [19] T. Jia, Z. Li, L. Ying, J. Jia, B. Fan, W. Zhong, F. Pan, P. He, J. Chen, F. Huang, Y. Cao, *Macromol. Rapid Commun.* 39 (2018) 1700765.
- [20] Y.J. Hwang, T. Earmme, S. Subramanian, S.A. Jenekhe, *Chem. Commun.* 50 (2014) 10801.
- [21] S. Liu, Y. Firdaus, S. Thomas, Z. Kan, F. Cruciani, S. Lopation, J.L. Bredas, P.M. Beaujuge, *Angew. Chem. Int. Ed.* 57 (2018) 531-535.
- [22] B. Fan, L. Ying, P. Zhu, F. Pan, F. Liu, J. Chen, F. Huang, Y. Cao, *Adv. Mater.* 29 (2017) 1703906.
- [23] D. Mori, H. Bente, I. Okada, H. Ohkita, S. Ito, *Energy Environ. Sci.* 7 (2014) 2939.
- [24] L. Gao, Z.-G. Zhang, L. Xue, J. Min, J. Zhang, Z. Wei, Y. Li, *Adv. Mater.* 28 (2016) 1884-1890.
- [25] C. Sun, F. Pan, H. Bin, J. Zhang, L. Xue, B. Qiu, Z. Wei, Z.-G. Zhang, Y. Li, *Nat. Commun.* 9 (2018) 743.
- [26] D. Zhu, X. Bao, Q. Zhu, C. Gu, M. Qiu, S. Wen, J. Wang, B. Shahid, R. Yang, *Energy Environ. Sci.* 10 (2017) 614.
- [27] X. Bao, Y. Zhang, J. Wang, D. Zhu, C. Yang, Y. Li, C. Yang, J. Xu, R. Yang, *Chem. Mater.* 29 (2017) 6766-6771.
- [28] D. Zhu, X. Bao, D. Ouyang, J. Wang, X. Yuan, Q. Wang, D. Zhou, S. Wen, R. Yang, *Nano Energy* 40 (2017) 495-503.
- [29] C. Cabanetos, A.E. Labban, J.A. Bartelt, J.D. Douglas, W.R. Mateker, J.M. Fréchet, M.D. McGehee, P.M. Beaujuge, *J. Am. Chem. Soc.* 135 (2013) 4656-4659.
- [30] L. Ye, S. Zhang, W. Zhao, H. Yao, J. Hou, *Chem. Mater.* 26 (2014) 3603-3605.
- [31] B. Fan, L. Ying, Z. Wang, B. He, X. Jiang, F. Huang, Y. Cao, *Energy Environ. Sci.* 10 (2017) 1243.
- [32] X. Xue, K. Weng, F. Qi, Y. Zhang, Z. Wang, J. Ali, D. Wei, Y. Sun, F. Liu, M. Wan, J. Liu, L. Huo, *Adv. Energy Mater.* 9 (2019) 1802686.
- [33] J. Liu, S. Chen, D. Qian, B. Gautam, G. Yang, J. Zhao, J. Bergqvist, F. Zhang, W. Ma, H. Ade, O. Inganäs, K. Gundogdu, F. Gao, H. Yan, *Nat. Energy* 1 (2016) 16089.
- [34] K. Dou, X. Wang, Z. Du, H. Jiang, F. Li, M. Sun, R. Yang, *J. Mater. Chem. A* 7 (2019) 958.
- [35] S. Shi, J. Yuan, G. Ding, M. Ford, K. Lu, G. Shi, J. Sun, X. Ling, Y. Li, W. Ma, *Adv. Funct. Mater.* 26 (2016) 5669-5678.
- [36] Z. Li, K. Jiang, G. Yang, J.Y. Lai, T. Ma, J. Zhao, W. Ma, H. Yan, *Nat. Commun.* 7 (2016) 13094.
- [37] C. Cui, W.-Y. Wong, Y. Li, *Energy Environ. Sci.* 7 (2014) 2276.
- [38] T. Zhang, G. Zeng, F. Ye, X. Zhao, X. Yang, *Adv. Energy Mater.* 8 (2018) 1801387.
- [39] B. Fan, P. Zhu, J. Xin, N. Li, L. Ying, W. Zhong, Z. Li, W. Ma, F. Huang, Y. Cao, *Adv. Energy Mater.* 8 (2018) 1703085.
- [40] N.B. Kolthe, H. Lee, D. Kuzuhara, N. Yoshimoto, T. Koganezawa, S. Jenekhe, *Chem. Mater.* 30 (2018) 6540-6548.
- [41] Y. Lin, F. Zhao, Y. Wu, K. Chen, Y. Xia, G. Li, S.K. Prasad, J. Zhu, L. Huo, H. Bin, Z.-G. Zhang, X. Guo, M. Zhang, Y. Sun, F. Gao, Z. Wei, W. Ma, C. Wang, J. Hodgkiss, Z. Bo, O. Inganäs, Y. Li, X. Zhan, *Adv. Mater.* 29 (2017) 1604155.
- [42] S. Liu, Z. Kan, S. Thomas, F. Cruciani, J.L. Brédas, P.M. Beaujuge, *Angew. Chem. Int. Ed.* 55 (2016) 12996-13000.
- [43] J. Li, Z. Liang, Y. Wang, H. Li, J. Tong, X. Bao, Y. Xia, *J. Mater. Chem. C* 6 (2018) 11015-11022.
- [44] Y.-J. Hwang, T. Earmme, B.A. Courtright, F.N. Eberle, S.A. Jenekhe, *J. Am. Chem. Soc.* 137 (2015) 4424-4434.
- [45] C. McDowell, M. Abdelsamie, M.F. Toney, G.C. Bazan, *Adv. Mater.* 30 (2018) 1707114.
- [46] W. Shen, W. Chen, D. Zhu, J. Zhang, X. Xu, H. Jiang, T. Wang, E. Wang, R. Yang, *J. Mater. Chem. A* 5 (2017) 12400-12406.